Convective Heat Transfer Coefficients and Mechanical Loss Evaluation of Oil Splashing in Direct Cooled Electrically Excited Hairpin Motors

Convective Heat Transfer Coefficients and Mechanical Loss Evaluation of Oil Splashing in Direct Cooled Electrically Excited Hairpin Motors.

Luca Boscaglia, *Member, IEEE* Yujing Liu, *Senior Member, IEEE*, Hasan Avsar, Junfei Tang, *Member, IEEE* and Massimo Galbiati.

***Abstract*—There in an increasing trend in the use of the direct oil cooling in electric motors for automotive because of the increasing demand of high power/torque density as well as overload capability. One of the most immediate solution is to fill the housing with some oil level and benefit of the heat transfer from the oil splashing. The mechanical losses coming from the rotor rotation are well known and they represent a significant challenge, especially at high speed and high oil level. Therefore, the derivation and prediction of these losses have not been properly investigated leading to a lack in the current literature. Moving Particles Simulation (MPS) method is used in Particleworks to calculate the mechanical losses caused by the oil viscosity and convective heat transfer coefficients (HTC) are extracted for a 250 kW Electrically Excited Synchronous Machine at different speeds and oil levels.**

***Index Terms*—Electric Motors, Direct Oil Cooling, Hairpin, Electrically Excited Synchronous Machine (EESM),Traction Motors, E-mobility, Automotive, Thermal, Heat Transfer Coefficient (HTC).**

I. Introduction

TRACTION motors for automotive demand very high power/torque density as well as wide speed range while keeping high efficiency along the whole driving cycle [1]–[5]. Since the motors require to be miniaturized, considering to keep constant the efficiency, the area of heat exchange decreases while the heat density increases [6]. This makes the temperature inside the motors rising with the increase of the power density of the machine and, therefore, better cooling performance are needed. The maximum temperature tolerated by the system is usually imposed by the thermal class of the coil insulation in the stator and/or the maximum operating temperature of the magnets inside the rotor in the case of PMSMs. Commonly, the windings cannot tolerate a higher temperature than 180°C [7] to avoid insulation damage, whereas the Nd magnets have 150°C temperature limit because of demagnetization [8]. Inefficient cooling system causes faster insulation degradation reducing the expected life of the machine [9]. Typically, a useful indication is that the temperature rise of 10°C over the material data sheet threshold is expected to reduce the insulation life of half [10]. In order to ensure the temperature below the limits, a good thermal strategy should solve the main challenges from all aspects including the reduction of the heat sources, the choice of optimal materials and the use of high performance cooling system. Electrical machines can be cooled down in approximately 4 ways [6]: (1) air-cooling were the air is moved by an external blower or a shaft-mounted fan [11], [12]; (2) water-cooling [13], [14] in which the water inside ducts at the interface between stator and housing (e.g. water jacket) and kept below certain temperature through an heat exchanger; (3) direct oil-cooling [15] where the high insulation properties of the oil are used to wet directly the conductors enhancing the heat transfer; (4) combined oil- and water- cooling [8] in which the water with the highest thermal conductivity is used to indirectly cool down the oil inside the motor. The best cooling performance are generally attributed to the combined oil- and water- cooling followed by direct oil-cooling, indirect oil-cooling and air-cooling. Although, the presence of two coolants requires more costs related to the installation and pressurization of two different cooling circuits. Direct oil cooling presents, instead several advantages:

- Oil is already used in automotive to lubricate rotating parts (e.g. bearings, gearbox), so the same oil circuit can be used to supply coolant to the motor and lubricants to mechanical rotating parts such as in Tesla motors [16].
- Oil is a good electric insulator and can be used in direct contact with electric active parts where water cooling is not sufficient due to the high thermal resistance between the winding and the water. In addiction, oil can enhance insulation where insulants are damaged due to manufacturing process, e.g. hairpin bending for end winding realization [17], preventing problems like partial discharges.
- The boiling point of oil is higher than water and this allows applications at more than 100°C.

This work is conducted by Chalmers University of Technology and financially supported by EU LONGRUN project (874972). Simulation tool ParticleWorks is provided and supported by EnginSoft SpA and Prometech Software Inc.

L. Boscaglia is with Chalmers University of Technology, Göteborg, 41296, Sweden (e-mail: luca.boscaglia@chalmers.se).

Y. Liu is with Chalmers University of Technology, Göteborg, 41296, Sweden (e-mail: yujing.liu@chalmers.se).

H. Avsar is with EnginSoft SpA, Italy (e-mail: h.avsar@enginsoft.com).

J. Tang is with Chalmers University of Technology, Göteborg, 41296, Sweden (e-mail: junfei.tang@chalmers.se).

M. Galbiati is with EnginSoft SpA, Italy (e-mail: m.galbiati@enginsoft.com).

- Cooling water should include corrosion inhibitor since can be corrosive to the machine parts and insulation, whereas oil spontaneously prevents corrosion [18].

There are different direct-oil cooling strategies that can be applied in order to cool down separately o conjointly the stator and rotor. In [8] an internal permanent magnets motor (IPM) is oil-cooled providing ducts in the housing for the stator cooling and hallow shaft for the rotor cooling. Compared with more traditional air cooling and water jacket, a 50% and 38% decrease respectively of the coil temperature is showed after 80 min of operation, whereas the temperature decreases by 42% and 10%. This cooling method is not mainly dependent from speed as the coolant is forced by pump pressurization through ducts. In [19] and [20], the spray cooling is investigated where oil is forced through tight orifices resulting in small droplets or thin film liquid which settle on the conductors surfaces [20]. Pais et al. [21] investigated about how the effectiveness of the spray is due to the molecules of droplets or film liquid that evaporate removing a large amount of heat at low temperature because of the latent heat of evaporation. This amount of heat is hard to quantify and it becomes larger the more the droplets are reduced in size. In [22] oil inside the rotor hollow shaft is investigated and an increase of the convective heat transfer coefficients (HTC) up to 600W/m2K is observed increasing the speed up to 5000 rpm with 3 l/min flow rate or increasing the flow rate up to 5 l/min with 3000 rpm. All the methods above mentioned consider direct cooling for the stator conductors whereas the rotor is cooled down decreasing the temperature of the lamination since they mostly take into consideration PMSMs. In this paper, 250 kW Electrically Excited Synchronous Machine for long haul transport is taken into account where active conductors are inserted in both stator and rotor. Since the rotor is not stationary, direct oil cooling can be challenging for the need of rotary junction in case of hallow shaft and because of the significant mechanical loss. Applications with flooded rotors at relatively high speed are main studied for pump applications and based on experiments [6] [23]. Simulations on oil splashing are usually not conducted since expensive and time consuming transient simulations using Finite Element Method (FEM) or Finite Volume Method (FVM) can take unreasonable times in the order of weeks to simulate some seconds of the oil path, especially at high speed. This leads to a void in the current literature for motor applications while the popularity of the oil direct cooling is largely increasing. The aim of this paper is to use Moving Particles Simulation (MPS) method to compute the oil particles tracking and evaluate the mechanical loss due to the hight viscosity torque applied to the rotor. In addition, the average convective heat transfer coefficient (HTC) along the surfaces of all the motor parts is calculated to evaluate the heat dissipation.

II. Calculation Method

The Moving Particle Simulation (MPS), formerly Moving Particle Semi-Implicit method, is a numerical method which deals with incompressible flow by discretizing continuum mechanics. The discretization of governing equations is handled with particle interaction models; therefore, mesh generation is not required and geometries are directly imported to the model for the creation of *Distance Funcions*.

A. Governing Equations

MPS method is governed by the Continuum Equation and Navier-Stokes equations respectively described by the following equations:

$$\frac{\partial \rho}{\partial t} = 0 \tag{1}$$

$$\frac{\partial \vec{\mathrm{u}}}{\partial t} = -\frac{\nabla P}{\rho} + \nu \nabla^2 \vec{\mathrm{u}} + \vec{\mathrm{g}} \tag{2}$$

where $\vec{\mathrm{u}}, P, \rho, \nu$ and $\vec{\mathrm{g}}$ are the velocity, pressure, density, kinematic viscosity and gravity acceleration respectively. The Heat Transfer equation is derived by the energy conservation law:

$$\frac{\partial e}{\partial t} = -\nabla(-\lambda_T \nabla T) \tag{3}$$

where e is the internal energy density, λ_T is the thermal conductivity, T the absolute temperature and $-\lambda_T \nabla T$ represents the heat flux. A summary of the algorithm steps of the MPS method is illustrated in Fig.1.

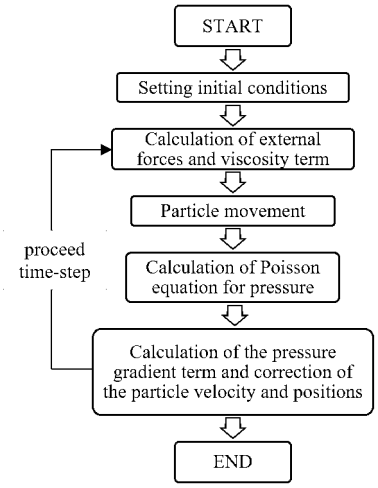

Fig. 1. Algorithm steps of the Moving Particles Simulation (MPS) method.

B. Effective Radius and Kernel (Weight) Function

In the MPS method particle interaction is defined with a certain distance called effective radius.

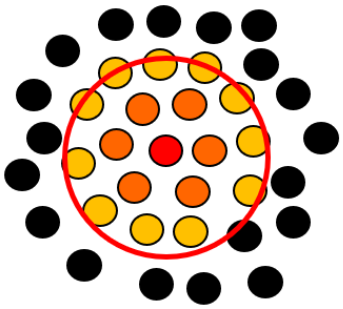

Fig. 2. Representation of effective radius.

In Fig. 2, red circle depicts the interaction region of the red particle which is the center point. Since orange and yellow particles are placed inside the interaction zone, they are called neighboring particles. On the other hand, black particles have no influence on the red particle due to the distance which is greater than effective radius. Therefore, as a referred particle, the red particle keeps information about neighboring particles only. In this manner, effective radius can be considered as sphere of influence calculated for every single particle in a 3-D simulation. The neighboring particles have quantitatively different influence on the reference particle. As the distance between red and one of the neighboring particles increases, the influence decreases exponentially. This phenomenon is represented by Kernel function. The interaction between the particles is weighted in accordance with the distance between two particles. The equation below is used for the weight function.

$$\omega(|\overrightarrow{r_{ij}}|) = \begin{cases} \frac{r_e}{|\overrightarrow{r_{ij}}|} - 1 & 0 \leq |r_{ij}| < r_e \\ 0 & |r_i j| \geq r_e \end{cases} \tag{4}$$

Subscripts of i and j represent particle numbers. r_e is the effective radius; in addition, $\overrightarrow{r_i j} = \overrightarrow{r_i} - \overrightarrow{r_j}$, where $\overrightarrow{r_i}$ is the position vector of particle i.

C. Particle Number Density

Particle number density is a unique and dimensionless parameter to the MPS method and it expresses the density of particle placement. This parameter is defined by:

$$n_i = \sum_{j \neq i} \omega\left(|\vec{r}_{ij}|\right) \tag{5}$$

The particle number density satisfies incompressibility condition and it represents the density of the fluid. The particle number density at the initial state, represented as n^0, is a fixed value of 54.32 for a 3-dimensional simulation and the particle placement at the initial state is arranged in an orthogonal grid with an initial distance of particle size.

D. Laplacian and Gradient Models

Viscosity and pressure terms are solved by Laplacian differential operator which is discretized as follows:

$$\left\langle \nabla^2 \phi \right\rangle_i = \frac{2d}{\lambda n^0} \sum_{j \neq i} \left(\phi_j - \phi_i\right) \omega\left(|\vec{r}_{ij}|\right) \tag{6}$$

$$\lambda = \frac{\sum_{j \neq i} |\vec{r}_{ij}|^2 \, \omega\left(|\vec{r}_{ij}|\right)}{\sum_{j \neq i} \omega\left(|\vec{r}_{ij}|\right)} \tag{7}$$

where d is the number of spatial dimensions. For example, in a 3-dimensional simulation, this number is taken as 3. The variables of particle i contribute to the other neighboring particles such as particle j by the Laplacian model. Quantity transfer is conserved since the quantity lost by particle i is just obtained by particle j [24]. The other differential operator is the gradient model which is used for calculating the velocity correction. As the Laplacian model, the gradient model is represented by using the weight function:

$$\langle \nabla \phi \rangle_i = \frac{d}{n^0} \sum_{j \neq i} \frac{\left(\phi_j - \phi_i\right) |\vec{r}_{ij}|}{|\vec{r}_{ij}|^2} \omega\left(|\vec{r}_{ij}|\right) \tag{8}$$

E. Viscosity Calculation

The effect of viscosity is calculated by the Laplacian model, and is time-integrated as shown below:

$$\vec{u}_i^* = \vec{u}_i^k + \frac{2d}{\lambda n^0} \Delta t \sum_{j \neq i} v_{ij} \left(\vec{u}_j^k - \vec{u}_i^k\right) \omega\left(|\vec{r}_{ij}^k|\right) \tag{9}$$

where ν_{ij} is the kinematic viscosity coefficient. Superscript *k* indicates the time step. Superscript * is indicative of a physical quantity at the stage where the explicit calculation has been completed.

F. Velocity and Pressure Calculation

Except pressure term, all terms in the Navier-Stokes equations are solved explicitly in the MPS method. Explicit calculation is shown below:

$$\frac{\vec{u}^* - \vec{u}^k}{\Delta t} = v \nabla^2 \vec{u}^k + \vec{g} \tag{10}$$

As velocity and viscosity terms are solved explicitly, Poisson equation for pressure is solved implicitly in order to satisfy incompressibility. Poisson equation is defined as follows:

$$\nabla^2 P^{k+1} = -\frac{\rho_{ij}}{\Delta t^2} \frac{n^* - n^0}{n^0} \tag{11}$$

From the calculated pressure, the pressure gradient is determined, and the velocity is corrected by the following equations:

$$\frac{\vec{u}^{k+1} - \vec{u}^*}{\Delta t} = -\frac{\nabla P^{k+1}}{\rho} \tag{12}$$

Correction of particle position and velocity by the pressure gradient is the final sub-step of an iteration in the MPS method.

G. Torque Calculation

A fluid particle, i, is accelerated by a rotating component of the geometry and this interaction creates a resistive force on the rotating component. The right-hand side of the Navier-Stokes equation, which is shown below, expresses pressure gradient force, viscous force and surface tension, respectively.

$$\frac{D\vec{u}_i}{Dt} = -\frac{\nabla P_i}{\rho_i} + v_i \nabla^2 \vec{u}_i + \vec{S}_i \tag{13}$$

Force acting on the rotating component is defined as

$$\vec{F}_i = -m_i \left(-\frac{\nabla P_i}{\rho_i} + v_i \nabla^2 \vec{u}_i + \vec{S}_i \right) \tag{14}$$

where m_i is the mass of the fluid particle. The torque T is calculated as follows.

$$T = \sum_i \vec{r}_i \times \vec{F}_i \tag{15}$$

where $\vec{r}_i$ is the relative position vector of the contact point between fluid particle and the rotating component with respect to the geometrical center of the rotating component.

H. Heat Transfer Coefficient Calculation

In the MPS method heat transfer coefficient is calculated by forced convection.Local Nusselt number Nu_x, local Reynolds number Re_x and Prandtl number Pr are expressed as follows.

$$Nu_x = hx/\lambda \tag{16}$$

$$Re_x = ux/v \tag{17}$$

$$Pr = \rho v c_p/\lambda \tag{18}$$

Where $h, x, \lambda, u, v, \rho, c_p, v$ represents heat transfer coefficient, distance from the beginning of the plate, thermal conductivity, average velocity, fluid density, specific heat and kinematic viscosity, respectively. The relation between the local Nusselt number and Reynolds number is defined by the following equations for both laminar and turbulent flow.

$$Nu_x = \begin{cases} 0.332\,\mathrm{Pr}^{1/3}\, Re_x^{1/2} & \text{Laminar flow} \\ 0.0296\,\mathrm{Pr}^{1/3}\, Re_x^{4/5} & \text{Turbulent flow} \end{cases} \tag{19}$$

III. Cooling and Modeling Strategy

The aim of this study is to investigate the mechanical losses produced by the interaction between the rotor and oil flow as well as the heat transfer derived by the oil motion. For this aim, a model of the motor is imported in Particleworks and computational fluid-dynamic simulations are executed at different speed and oil levels using MPS method.

A. Case Study Machine

The motor considered in this study is an high power density 250 kW Electrically Excited Synchronous Machine (EESM) for truck application. The rotor field winding are wounded around the 8 salient poles whereas the stator winding are made of 4 layers hairpin. The coolant used is oil provided by ExxonMobil. The machine dimensions and the oil properties are summarized in Table I and Table II respectively.

TABLE I
MACHINE PARAMETERS.

Parameter	Value	Unit
Stator Outer Diameter	230	mm
Stator Inner Diameter	170	mm
Rotor Outer Diameter	168	mm
Machine Length	130	mm
Number of Stator Hairpin Layers	4	
Number of Rotor Poles	8	
Machine Maximum Power	250	kW
Machine Maximum Torque	500	Nm

TABLE II
OIL PROPERTIES.

Parameter	Value	Unit
Density	800	kg/m^3
Thermal Conductivity	0.145	W/mK
Specific Heat	1845	J/kgK
Kinematic Viscosity	0.00000128	m^2/s
Surface Tension Coefficient	0.03	N/m
Machine Maximum Power	250	kW
Machine Maximum Torque	500	Nm

B. Model Strategy

Given the geometric symmetry, only half of the motor is imported in the model and used for the simulations. As consequence, all the results presented should take into account a factor of 2. The case study motor is filled with different oil levels: 0.200 L, 0.300L, 0.500 L, 0.700L and 1.100 L as shown partially in Fig.3. The influence of the air is considered to affect the oil path mostly at high speed and low liquid level, for this reason the air is simulated for the cases with 0.200 and 0.300 oil liters only. At high oil level (more than 0.300 liters), when the oil is touching a larger part of the rotor and field winding surface, the oil motion is mostly dependent by the rotation of the solid rotating parts, as demonstrated and shown in Section IV. The model does not require the meshing of the solid parts, for this reason the complexities of the real motor, in particular the shape of the hairpin end windings, can be imported directly. In order to reduce the computational time, the explicit solvers are activated for both pressure and viscosity calculation. For the pressure prediction, the speed of sound should be estimated and can be considered about five times the rotor tangential velocity.

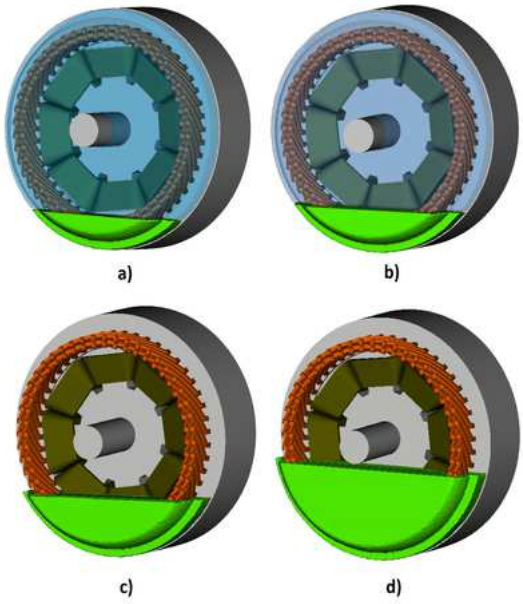

Fig. 3. Oil levels inside the machine considered for the computations: a) 0.200L of oil + air; b) 0.300L of oil + air; a) 0.500L of oil; d) 1.00L of oil

C. Time step estimation

For all the simulations, a particle size of 1.2 mm is considered to allow all the particles to pass inside the space between the hairpin layers. In order to avoid divergence, the velocity limiter is activated during the simulations and a proper initial time step is set. The maximum velocity of the particles can be calculated as the maximum tangential velocity of the rotor obtained multiplying the rotor radius r_r and the angular speed of the rotor ω_r:

$$\mathrm{U_{max}} = \omega_\mathrm{r}\, \mathrm{r_r} \tag{20}$$

Considering the oil properties, three different time steps can be defined that are essential for the simulation stability:

$$v_e = \begin{cases} \Delta t = \frac{l}{U_{\max}}, & Inertial\ time\ step \\ \Delta t = \frac{l^2}{2v}, & Viscous\ time\ step \\ \Delta t = \sqrt{\frac{\rho l^3}{2\pi\sigma}}, & Surface\ Tension\ time\ step \end{cases} \tag{21}$$

where ρ is the oil density, σ is the surface tension coefficient, ν the kinematic viscosity and l the particle size. The global time step should be lower or equal to the lowest of the time steps in (31) in order to have numerical stability.

IV. Air Ventilation

With the aim to understand the effect of the air ventilation on the oil splashing and, as consequence, on the mechanical losses and dissipation of the heat, simulations are conducted at 1000 rpm and 0.500 liters comparing three cases:

- only oil splashing calculated with MPS method;
- multi-phase simulation with both oil and air using MPS method.
- multiphase simulation with both oil and air combining MPS and Finite Volume Method (FVM): the Moving Particles Method is used for the oil calculation instead the FVM is used for the air simulation.

In Fig. 5 it is possible to observe that no significant differences are emerged from the study in terms of oil path since the effect of the air ventilation on the oil is not notable. In addition, in Fig. 6 very similar values are obtained for the viscosity torque applied by the oil to the rotor for the three cases. As results, the air will be taken into account for the simulations only for very low oil level, where the rotor lamination and the field winding partially touch the oil and the ventilation affects has a huge part in the oil spreading.

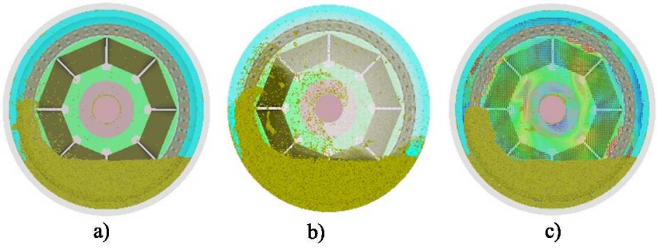

Fig. 4. Oil splashing at 1000 rpm considering three different scenarios: a) only oil simulation with MPS; b) both oil and air simulated with MPS; c) oil simulated with MPS and air with FVM.

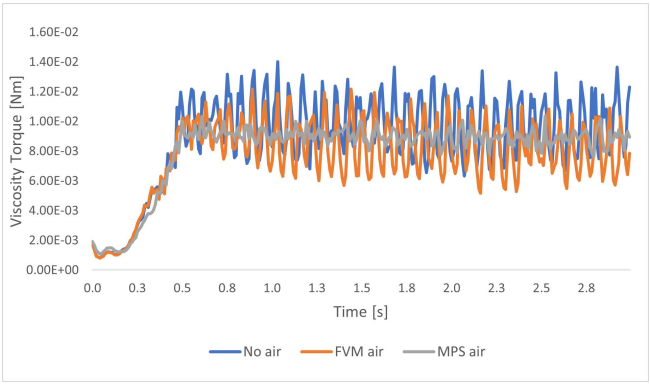

Fig. 5. Viscosity Torque applied to the rotor for three scenarios: 1) with no air simulated; 2) air simulated using FVM; 3)Air simulated with MPS method.

V. Simulation Results

The results for 2 s of simulation are presented for a speed range from 500 rpm up to 10000 rpm and for oil level from 0.200 liters to 1.00 liters in Fig. 6, Fig.7 and Fig.8. In Fig. 7, the oil splashing is illustrated at 1000 rpm, 5000 rpm and 10000 rpm from the left to the right and for increasing oil level from the top to the bottom. In case of very low oil level (0.200 L), the oil is standing mostly at the bottom of the housing whereas it starts reaching the hairpin winding at higher speed (5000 rpm and 10000 rpm). Increasing the rotor speed, the turbulence increases enhancing the diffusion of the oil along the stator lamination and hairpin layers. It can be noticed that the centrifugal forces produced by the

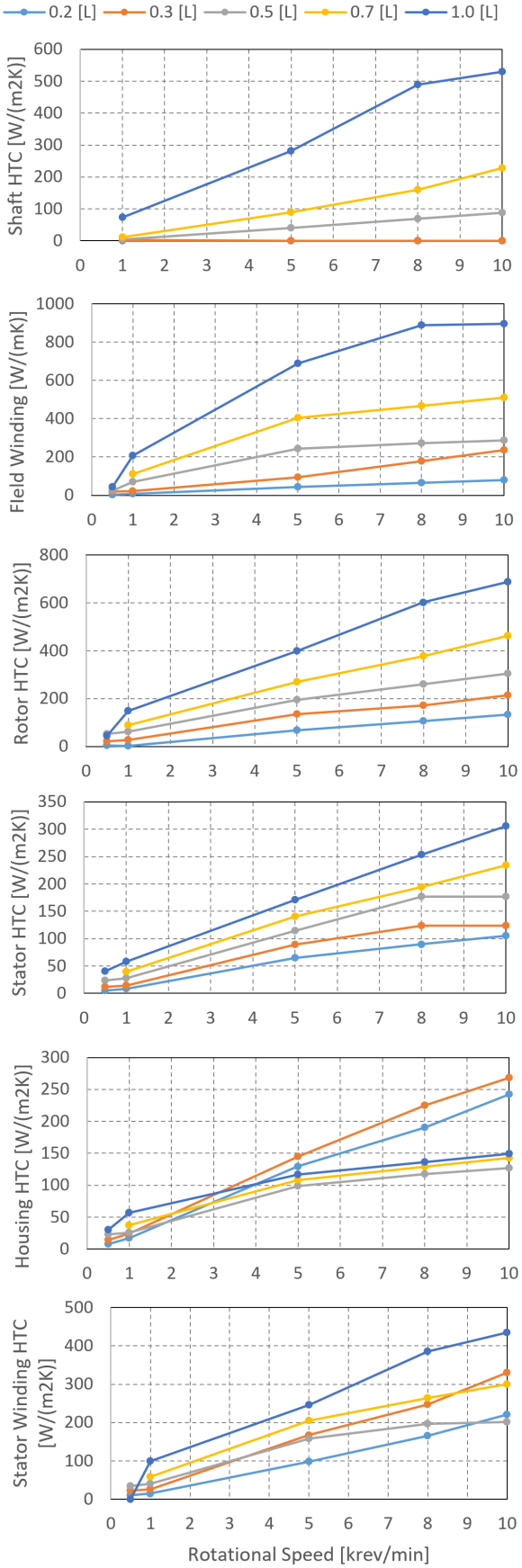

Fig. 6. Results of convective Heat Transfer Coefficients for the different parts of the motor.

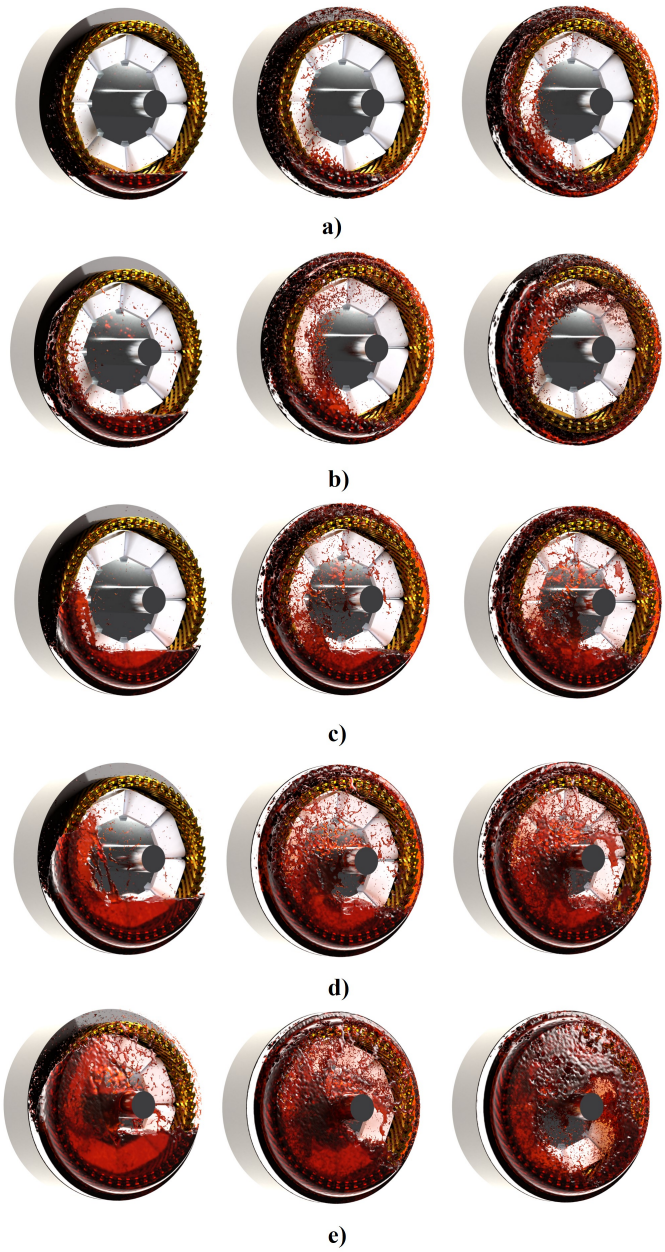

Fig. 7. Oil Splashing inside the motor at three rotor speeds 1000 rpm, 5000 rpm and 10000 rpm (from left to right) and different oil levels: a) 0.200 L; b) 0.300 L; c) 0.500; L d) 0.700L; e) 1.00 L.

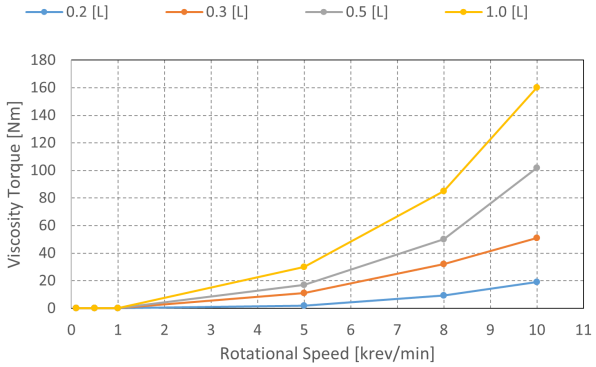

Fig. 8. Viscosity Torque due the interaction between rotor rotation and oil at different speed and for several oil levels.

rotor tangential acceleration at high speed lead the oil to the stator outer diameter also at very low level, bringing benefit for the heat dissipation also with only 0.2 liters. In Fig. 6 the values of the convective heat transfer coefficients are plotted for all the motor parts. Observing the HTC for shaft, field winding, rotor and stator lamination, a pseudo-linear trend can be observed reaching in some cases a slight saturation. This means that increasing the oil level and the rotor speed, the dissipated heat rises. The only exception is noticed for the stator winding and housing since similar values are obtained at both low and high oil volume. This can be explained considering that for all the different levels of oil, the coolant is anyway mostly accumulated in the peripheral area of the machine due to the centrifugal forces due to the rotor rotation. In Fig. 8 the torque produced by the viscosity of the oil is shown for values of the machine speed from 500 rpm to 10000 rpm and oil volume from 0.200 L to 1.00 L. As confirmation, this cooling strategy demonstrates the drawback of very high mechanical losses at high speed following a parabolic curve increasing the rotor angular velocity. For values of speed under 1000 rpm, the mechanical losses can be considered acceptable for almost all the oil level since no significant load torque is applied to the rotor lamination. Increasing the speed above 1000 rpm, a significant difference is noticed between the different amounts of coolant reaching, at maximum speed of 10000 rpm and oil level of 1.0L, a viscosity torque equal to the 32% of the maximum torque.

VI. Conclusion

In this paper, the effect of the oil splashing on the heat dissipation and the mechanical losses for an Electrically Excited Synchronous Machine are considered. MPS has demonstrated high calculation performance and fast computation time compared to Finite and Volume Element Methods moving the computation time of transient fluid-dynamic from days to hours with a commercial GPU. The effect of the oil splashing can lead to significant advantages in terms of dissipation of heat whereas the mechanical losses can be very high. For this reason, a proper cooling strategy considering an active control of the liquid depending on the machine speed should be implemented.

References

[1] W. Hua, H. Zhang, M. Cheng, J. Meng, and C. Hou, "An outer-rotor flux-switching permanent-magnet-machine with wedge-shaped magnets for in-wheel light traction," *IEEE Transactions on Industrial Electronics*, vol. 64, no. 1, pp. 69–80, 2017.

[2] S.-U. Chung, S.-H. Moon, D.-J. Kim, and J.-M. Kim, "Development of a 20-pole–24-slot spmsm with consequent pole rotor for in-wheel direct drive," *IEEE Transactions on Industrial Electronics*, vol. 63, no. 1, pp. 302–309, 2016.

[3] X. Liu, H. Chen, J. Zhao, and A. Belahcen, "Research on the performances and parameters of interior pmsm used for electric vehicles," *IEEE Transactions on Industrial Electronics*, vol. 63, no. 6, pp. 3533–3545, 2016.

[4] P. Ponomarev, M. Polikarpova, O. Heinikainen, and J. Pyrhönen, "Design of integrated electro-hydraulic power unit for hybrid mobile working machines," in *Proceedings of the 2011 14th European Conference on Power Electronics and Applications*, 2011, pp. 1–10.

[5] J. Miller and D. Howell, "The ev everywhere grand challenge," *World Electric Vehicle Journal*, vol. 6, pp. 1008–1013, 12 2013.

[6] S. Sugimoto and D. Kori, "Cooling performance and loss evaluation for water- and oil-cooled without pump for oil," in *2018 XIII International Conference on Electrical Machines (ICEM)*, 2018, pp. 1136–1141.

[7] T. Davin, J. Pellé, S. Harmand, and R. Yu, "Experimental study of oil cooling systems for electric motors," *Applied Thermal Engineering*, vol. 75, pp. 1–13, 2015. [Online]. Available: https://www.sciencedirect.com/science/article/pii/S1359431114009314

[8] K.-H. Lee, H.-R. Cha, and Y.-B. Kim, "Development of an interior permanent magnet motor through rotor cooling for electric vehicles," *Applied Thermal Engineering*, vol. 95, pp. 348–356, 2016. [Online]. Available: https://www.sciencedirect.com/science/article/pii/S1359431115012582

[9] B. Jiang, X. Huang, Y. Liu, and S. Nategh, "Accelerated destructive experiment design of motor stator winding insulation systems," in *2021 IEEE Workshop on Electrical Machines Design, Control and Diagnosis (WEMDCD)*, 2021, pp. 225–230.

[10] K. G. Toliyat, H.A., "Handbook of electric motors," *(CRC Press, Boca Raton, FL*, 2004.

[11] L. Boscaglia, F. Bonsanto, A. Boglietti, S. Nategh, and C. Scema, "Conjugate heat transfer and cfd modeling of self-ventilated traction motors," in *2019 IEEE Energy Conversion Congress and Exposition (ECCE)*, 2019, pp. 3103–3109.

[12] L. Boscaglia, A. Boglietti, S. Nategh, F. Bonsanto, and C. Scema, "Numerically based reduced-order thermal modeling of traction motors," *IEEE Transactions on Industry Applications*, vol. 57, no. 4, pp. 4118–4129, 2021.

[13] G. Venturini, G. Volpe, and M. Popescu, "Slot water jacket cooling system for traction electrical machines with hairpin windings: Analysis and comparison," in *2021 IEEE International Electric Machines Drives Conference (IEMDC)*, 2021, pp. 1–6.

[14] L. Ye, F. Tao, W. Xuhui, and L. Qi, "Experimental investigation of heat transfer and resistance characteristics of the motor water jackets," in *2014 IEEE Conference and Expo Transportation Electrification Asia-Pacific (ITEC Asia-Pacific)*, 2014, pp. 1–3.

[15] L. Ye, F. Tao, L. Qi, and W. Xuhui, "Experimental investigation on heat transfer of directly-oil-cooled permanent magnet motor," in *2016 19th International Conference on Electrical Machines and Systems (ICEMS)*, 2016, pp. 1–4.

[16] Z. ZI-CHAO, S. QIANG, and B. AHMED, "Innovative design of the cooling topologies for electric vehicle motors," *IOP Conference Series: Materials Science and Engineering*, vol. 533, no. 1, p. 012021, may 2019. [Online]. Available: https://doi.org/10.1088/1757-899x/533/1/012021

[17] F. Wirth, T. Kirgör, J. Hofmann, and J. Fleischer, "Fe-based simulation of hairpin shaping processes for traction drives," in *2018 8th International Electric Drives Production Conference (EDPC)*, 2018, pp. 1–5.

[18] R. Pechanek and L. Bouzek, "Analyzing of two types water cooling electric motors using computational fluid dynamics," 09 2012, pp. LS2e.4–1.

[19] M. H. Park and S. C. Kim, "Thermal characteristics and effects of oil spray cooling on in-wheel motors in electric vehicles," *Applied Thermal Engineering*, vol. 152, pp. 582–593, 2019. [Online]. Available: https://www.sciencedirect.com/science/article/pii/S1359431118362756

[20] J. Kim, "Spray cooling heat transfer: The state of the art," *International Journal of Heat and Fluid Flow*, vol. 28, no. 4, pp. 753–767, 2007, including Special Issue of Conference on Modelling Fluid Flow (CMFF'06), Budapest. [Online]. Available: https://www.sciencedirect.com/science/article/pii/S0142727X06001639

[21] T. D. C. L. M. E. Pais, M., "High heat flux, low superheat evaporative spray cooling," 1989.

[22] R. Wang, X. Fan, D. Li, and R. Qu, "Comparison of two hollow-shaft liquid cooling methods for high speed permanent magnet synchronous machines," in *2020 IEEE Energy Conversion Congress and Exposition (ECCE)*, 2020, pp. 3511–3517.

[23] A. Al-Timimy, P. Giangrande, M. Degano, Z. Xu, M. Galea, C. Gerada, G. Lo Calzo, H. Zhang, and L. Xia, "Design and losses analysis of a high power density machine for flooded pump applications," *IEEE Transactions on Industry Applications*, vol. 54, no. 4, pp. 3260–3270, 2018.

[24] S. Koshizuka and Y. Oka, "Moving-particle semi-implicit method for fragmentation of incompressible fluid," *Nuclear Science and*

Engineering, vol. 123, no. 3, pp. 421–434, 1996. [Online]. Available: https://doi.org/10.13182/NSE96-A24205

VII. Biographies

Luca Boscaglia (S'17-M'19) received his B.Sc. and M.Sc. in electrical engineering respectively from University of Napoli Federico II and Politecnico di Torino, in Italy. He did his master thesis at ABB Traction Motors in Västerås, Sweden, about thermal and CFD modeling of electric traction motors for railway. He joined ABB Low Voltage Motors and Generators in Vittuone in 2019, in Milan, working in RD mostly on thermal design and fluid dynamic computations of electrical machines. In 2020, he started the PhD at Chalmers University of Technology in Göteborg, Sweden, on Electrical Machine Design for Vehicle Applications

Yujing Liu (SM'12) received B.Sc., M.Sc. and Ph.D. degrees in electrical engineering from Harbin Institute of Technology, Harbin, China, in 1982, 1985, and 1988, respectively. In 1996-2013, he worked in ABB Corporate Research, Västerås, Sweden. Since 2013, he is a professor on electrical power engineering in Chalmers University of Technology. Gothenburg, Sweden. His interest includes research on motors, converters, and wireless charging for electric vehicles, generators and power electronics for tidal power conversion, and high efficiency machines for energy saving in industrial applications. Yujing Liu is a senior IEEE member and a member in Swedish Standard Committee on Electrical Machines.

Hasan Avsar Hasan Avsar was born in Manisa, Türkiye on the 6th of October, 1990. He graduated from Istanbul Technical University. His employment experience included FIGES Engineering and TUSAS Engine Industries. His special fields of interest included Computational Fluid Dynamics, Aerodynamics and Multi-objective Optimization. Currently he is working as a CFD Engineer at EnginSoft, in Bergamo, Italy.

Junfei Tang (S'16–M'22) received the B.Eng. degree in electrical engineering from Jiangsu University, Zhenjiang, China, in 2013, and the M.Sc and Ph.D degrees in electric power engineering from Chalmers University of Technology, Gothenburg, Sweden, in 2016 and 2021 respectively. Now he is a postdoctoral researcher in electric machines and power electronics in Chalmers University of Technology. Junfei Tang was acknowledged as a star reviewer for 2020 by the IEEE Power Energy Society and the Editorial Board of the IEEE Transactions on Energy Conversion.

Massimo Galbiati Massimo Galbiati was born in Mian (Italy) in 1973. He graduated from the Politecnico di Milano. His employment experience included ENI and EnginSoft. His special field of interest included Finite Volume CFD, optimization methods and particle-based CFD. Currently he is in charge of the particle-based CFD team at EnginSoft in Bergamo (Italy)